Optimizing Processes and Materials for Flip Chip Reliability

Karl-Friedrich Becker and Tom Adams

Careful material selection can yield FC assemblies with better reliabilities than some surface-mount components.

The overall attractiveness of the flip chip design has been enhanced in the past few years by continued improvements in achievable reliability and in production yield. As a result, flip chips are now commonly used in advanced high-volume products such as cell phones and global positioning system (GPS) devices and in critical-reliability devices such as cardiac pacemakers.

To show the high potential of state-of-the-art underfill materials to achieve the highest yield and reliability in specific production environments, a study was undertaken at Fraunhofer IZM to investigate five commercially available, advanced underfill materials. The study used techniques previously developed or refined at Fraunhofer IZM, including the use of video equipment to permit the direct microscopic visualization of underfill flow rates and the use of an acoustic micro imaging system to nondestructively image material inhomogeneities. These techniques were used to detect voids and irregular filler particle distribution.

Additionally, the influence of various substrate base materials, solder mask types and geometries on the underfill materials was investigated via acoustic micro imaging. To correlate actual reliability with conclusions drawn about materials and processes, accelerated aging tests were performed.

Acoustic micro imaging was also used to nondestructively image the underfill features during this stage of the study. The overall flip chip geometry makes acoustic imaging especially useful because the silicon die itself is nearly transparent to ultrasound.

Part of the impetus for this study was the continuous upgrading of underfill materials themselves by manufacturers. Chip sizes have become larger (15 mm+), while the underchip gap has become thinner (<40 microns). These changes have dictated improved resin/hardener systems having minimum reaction time and low viscosity, as well as increasingly smaller filler particles.

The five materials investigated here appeared capable of meeting the multiple demands of profitable flip chip processing, including high yield, high throughput, low cost, suitability for large integrated circuits (ICs), fine pitch and insensitivity to printed circuit board (PCB) topography. These five materials were also selected because they appear to have low viscosity, short cure times, minimal air entrapment, strong adhesion and post-cure thermo-mechanical properties that would promote long-term reliability.

Previous experience and finite element modeling (FEM) have suggested that underfill materials in this application should have a Young's modulus between 2 and 12 MPa, a coefficient of thermal expansion (CTE) between 20 ppm/°K and 40 ppm/°K, a glass transition (Tg) about 15° K above maximum use temperature and a viscosity below 1 Pa*s at an underfilling temperature between 70° and 90°C. The five materials selected met all of these criteria.

To further test the behavior of these materials, three types of solder mask materials were used in the study. Material properties of the underfill materials are shown in Table 1, while those of the solder mask materials are shown in Table 2.

After the material properties had been determined, the flow properties of the underfill materials were investigated using both flow module test

The five materials investigated here appeared capable of meeting the multiple demands of profitable flip chip processing.

		Underfiller				
	Unit	A	B	C	D	E
Liquid Properties						
Viscosity @ 25° C	[Pa*s]	12	10	8	20	1
Viscosity @ 70° C	[Pa*s]	0.59	0.61	0.19	0.73	0.04
Viscosity @ 80° C	[Pa*s]	0.39	0.51	0.17	0.47	0.09
Density ρ	[g/cm³]	1.8	1.7	1.52	1.8	1.4
Filler Content	[wt%]	68	62	40	70	30
Max. Particle Size	[μm]	12	15	10	8	5
Surface Tension γ @ 25°C	[mN/m]	33	39	40	32	43
Contact Angle θ @ 25°C on Glass	[°]	33	35	46	39	44
Cos θ		0.84	0.82	0.69	0.78	0.72
CPP ϕ @ 70°C on Glass	[mm/s]	16	18	48	12	242
Processing						
Shelf Life @ -40°C	[months]	9	9	6	5	6
Pot Life @ 25°C	[days]	2	1/3	>1/3	3	n.a.
Gelation Time	[min]	n.a.	6 @ 121°C	n.a.	n.a.	2.7@ 150°C
Processing Temperature	[°C]	70-100	70-90	70-100	70-100	70-80
Recommended Cure Profile		30 min @ 165°C	10 min @ 160°C	5 min @ 150°C	15 min @ 150°C	1 h @ 150°C
Cured Properties						
Thermal Conductivity	[W/(mK)]	0.45	0.41	0.32	0.48	0.31
Glass Transition Temperature DSC	[°C]	140	n.a.	135	n.a.	155
TMA	[°C]	158	144	101	113	160
Coefficient of Thermal Expansion a1	[10⁻⁶/K]	26	28	40	23	40
a2	[10⁻⁶/K]	87	104	133	84	147
Flexural Modulus	[GPa]	10.3	7.6	2.8	10	3.5
Tensile Modulus	[GPa]	5.5	3.2	2.8	n.a.	n.a.
Linear Shrinkage	[%]	0.14	n.a.	3	n.a.	n.a.
Water Uptake	[wt%]	0.47	0.70	1.77	0.59	0.83
Extractable Ionic Content Cl-	[ppm]	5	20	30	n.a.	15
Na+	[ppm]	5	5	1	n.a.	2
K+	[ppm]	n.a.	5	1	n.a.	1

Material Property determined at Fraunhofer IZM. Calculated Material Property.

TABLE 1: Material properties of flip chip underfillers studied.

Property	Unit	SM-1	SM-2	SM-3
Solder Mask Thickness	[μm]	49	15	22
Solder Mask Opening Diameter	[μm]	124	109	138
Solder Mask Roughness	[μm]	0.3	0.2	0.3
Surface Energy Initial State	[mN/m]	31	38	29
Surface Energy After Reflow	[mN/m]	23	28	26

TABLE 2: Properties of solder mask materials.

vehicles and actual flip chip assemblies. The latter used an FR-4 substrate and held six 10 mm x 10 mm flip chips, peripherally bumped with 300μ pitches. Each flip chip die included a daisy chain pattern for rapid resistance measurements. The solder used was eutectic tin-lead (Sn-Pb) on an electroless nickel (Ni) underbump metallization. Bump diameter before assembly was about 100 microns and, after assembly, about 80 microns. The final gap varied with the thickness of the solder mask. A state-of-the-art no-clean flux was used, and reflow was carried out in an N^2 atmosphere with a maximum temperature of 230°C.

The flow module test vehicles consisted of a glass slide adhesively fastened to a substrate. At one end, spacer particles between the glass and the substrate determined the height of the gap. The test vehicles were heated to the desired process temperature (typically 70°C to 90° C), and an underfill material was dispensed at the end of the test vehicle. Video equipment recorded underfill flow speed. Post-cure, an acoustic micro imaging system inspected the optically opaque underfill nondestructively for voids and agglomerations of filler particles. Where acoustic imaging showed a void or an agglomeration, the test vehicle was cross-sectioned for optical or scanning electron microscope (SEM) imaging.

Analysis of the Five Underfill Materials

Differential scanning calorimetry, dynamic-mechanical analysis, thermo-mechanical analysis, thermo-gravimetrical analysis, rheology, tensiometry and atomic force microscopy were used to perform a thorough analysis of the five underfill materials.

Material A had a mid-range viscosity (0.59 Pa•s at 70° C) and a mid-range surface tension (33 mN/m). The filler content was fairly high (70% by weight), and the 12 micron particles were fairly large. Thermo-mechanically, this material was rather stiff (Young's modulus 10 GPa). It had a low CTE (26 ppm/°K) that was close to the CTE of the solder.

Material B was similar in its viscosity (0.61 Pa*s at 70° C) and surface tension (39 mN/m) to Material A. Filler content was 62% by weight, and the particle size of 15 microns was the largest of the five materials. The Young's modulus was 7.6 GPa, and the CTE was 28 ppm/°K.

Material C had a low viscosity (0.19 Pa*s at 70° C), and its surface tension of 40 mN/m was close to that of Material B. Filler content was a low 40% of weight, and particle diameter was 10 microns. Thermo-mechanically, Material C was rather soft, having a Young's modulus of 2.8 GPa. The CTE was quite high at 40 ppm/°K. Material C had a humidity uptake (1.77 wt%) at least double that of the four other materials. Note that humidity uptake may or may not be related to filler content; Material E had a similar filler content but a humidity uptake of only 0.83 wt%.

Material D had the highest viscosity (0.73 Pa*s at 70° C) and the lowest surface tension (32 mN/m). It also had the highest filler content (70 wt%) and fairly small particles (8 microns). It had a Young's modulus of 10 GPa like Material A. Because of the high filler content, it had a low CTE of 23 ppm/°K, which closely matched the CTE of eutectic SnPb solder.

Material E had the lowest viscosity (0.04 Pa*s at 70° C) and the highest surface tension (44 mN/m). It also had the lowest filler content (30 wt%) and the smallest particles (5 microns). Relatively soft, it had a Young's modulus of 3.5 GPa. The CTE, like that of Material C, was 40 ppm/°K. Material E also had the highest coefficient of planar penetration (CPP)—244 mm/s; the next highest CPP was 48 mm/s for Material C. The very high CPP

was primarily a function of the very low viscosity of this material.

Solder Mask Materials

Three solder mask (SM) materials were used in the study. Atomic force microscopy showed little difference in surface roughness among the three materials. Surface energy of the solder mask materials was measured by the sessile drop method before and after reflow. In the initial state, strong variations in surface energy occurred, but these variations were greatly diminished after reflow.

The geometry of the solder mask, then, appeared to be more important in influencing underfill flow. SM 1 was 2.5 to 3 times thicker than the other two materials; as a consequence, the underfill gap was about 65 microns for SM 2, about 60 microns for SM 3 and only 30 microns for SM 1.

Flow Testing

Empirical testing of flow behavior was carried out with the flow module test vehicles and the actual flip chip assemblies described earlier. A video camera recorded the flow process in the test vehicle; post-cure, both the test vehicles and the flip chip assemblies were inspected by acoustic micro imaging (Figure 1), followed by physical sectioning where significant defects were present.

Material A, which had a CPP of 16 mm/s, flowed at a slow rate and was susceptible to particle clumping. In the flow modules, clumping of particles occurred after only 1.5 mm of travel; in the flip chip module, clumping occurred after 5 mm. Used with the relatively thick SM 1, Material A gave a gap of only 30 microns, and voids formed near the bumps. Cross sectioning showed no settling of the particles; particle distribution was uniform vertically across the gap. Overall, the processability of Material A was judged to be only poor to fair.

The behavior of Material B was like that of Material A, primarily because the CPP (18 mm/s) was similar. Clumping of particles occurred after 1.5 mm of flow in the flow modules and after 5 mm in the flip chip module, although clumping was less pronounced than for Material A.

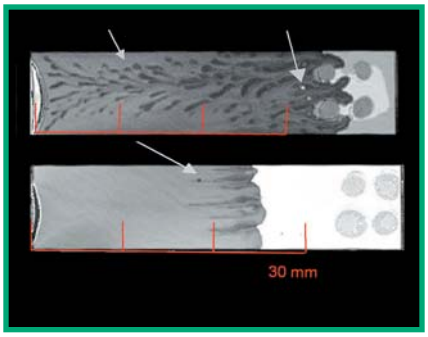

FIGURE 1: Post-cure C-SAM acoustic image of flow module testing of Materials A and C. Direction of flow of the underfill is from the left. Arrows point out dark regions (particle agglomeration) and bright regions (trapped air).

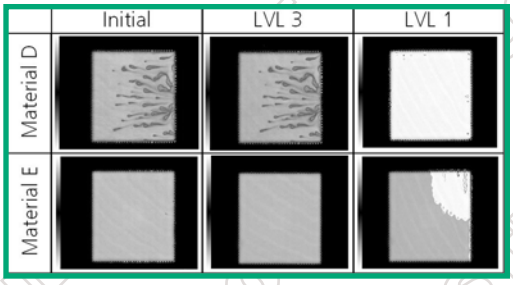

FIGURE 2: C-SAM acoustic images of flip chip assemblies for Materials D and E during popcorn testing. At right, Material D is 100% delaminated, while Material E is 30% delaminated.

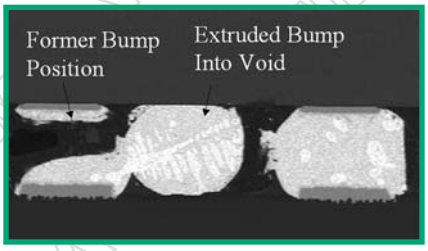

FIGURE 3: Cross section of an assembly after popcorn testing, showing the extrusion of the bump material into an adjacent void.

Some voids occurred in the flow modules, but only after 30 mm of travel. Voids were also observed in the flip chip modules, but only around the bumps when SM 1 was used. Vertical distribution of the particles was uniform. Material B was judged to have fair processability.

Material C, having a much higher CPP of 48 mm/s, flowed rapidly for up to 10 mm in the flow modules; at this point the flow front became ragged. After 18 mm of travel, minor clumping of particles occurred but no air entrapment. In the flip chip modules, no particle clumping took place, and voids occurred only adjacent to the bumps in SM 1 modules. Cross sectioning showed even distribution of particles vertically. Overall, Material C was the second best material tested.

With a CPP of 12 mm/s, Material D flowed slowly and unevenly. Particle clumping on a scale similar to Material B began after only 1.5 mm of travel in the flow modules, and air entrapment occurred after 20 mm. In the flip chip modules, particle clumping began after about 3 mm of travel, along with minor air entrapment. Voids also formed near the bumps in SM 1 modules. Particle distribution was uniform across the gap. Overall processability was poor.

Material E had the lowest viscosity of the five materials and a CPP of 242 mm/sec. Clumping of particles occurred after 20 mm of travel, but no air was trapped by the flow front. In the flip chip modules no particle clumping and only very minor air entrapment near the bumps in the SM 1 modules occurred. Cross sectioning showed that particle distribution across the gap was uniform. This material had the highest overall processability.

Reliability Testing

The assemblies were tested for popcorn cracking according to JEDEC Std. 20, Levels 1 and 3. This testing typically caused delaminations (Figure 2), all of which resulted in electrical failures when the bump material moved into the gap created by the delamination (Figure 3).

Pressure cooker testing was carried out at 121° C and 100% relative humidity (RH). The typical failure was a delamination between the chip's passivation layer and the underfill. Not all of these delaminations resulted in immediate electrical failures, probably because humidity testing puts little mechanical load on the assemblies. But delaminated assemblies subjected to thermal cycling tended to fail after only a few cycles (Figures 4, 5).

Thermal cycling itself typically caused a delamination between the chip and the

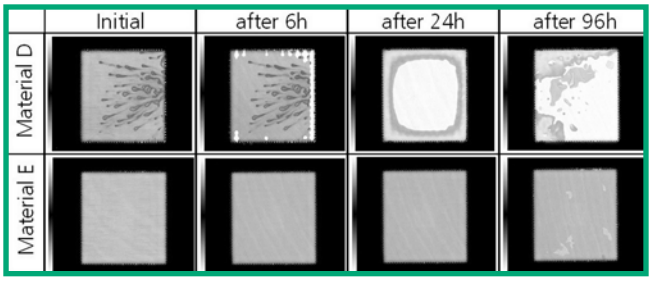

FIGURE 4: C-SAM acoustic images of test assemblies for Materials D and E during the course of pressure cooker testing. In Material D, delaminations began after six hours; in Material E, delaminations are just beginning after 96 hours.

underfill, as well as resulting cracks in solder bumps and electrical failure (Figure 6). In addition, a few cracks were found at the interface between the substrate and the solder bumps. The cracks extended into the substrate.

The five underfill materials behaved as follows in reliability testing:

Material A

No delaminations were noted after Level 3 testing, but full delaminations and electrical failure occurred after Level 1. Peripheral delaminations were noted after only six hours in the pressure cooker; full delaminations and partial electrical failure occurred after 96 hours. In thermal cycling, delaminations occurred from SM 1 and SM 3 after 250 cycles and after 1,000 cycles from SM 2. Electrical failures occurred only after 1,500 cycles for SM 3.

Material B

No delaminations were noted after Level 3 testing, but full delaminations and electrical failure occurred after Level 1. Peripheral delaminations were noted after only six hours in the pressure cooker; full delaminations occurred with all three solder mask types; electrical failure happened after 24 hours for SM 3 and after 96 hours for SM 2. In thermal cycling, delaminations occurred from SM 1 after 500 cycles and after 1750 cycles from SM 2 and SM 3. Electrical failures happened only after 2000 cycles for SM 2.

Material C

No delaminations were noted after Level 3 testing, but full delaminations and electrical failure occurred after Level 1.

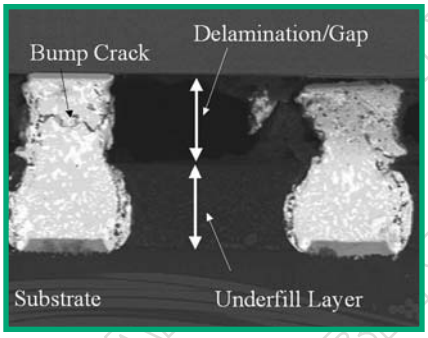

FIGURE 5: Cross-sectional view of an assembly using Material C after pressure cooker testing showed a significant gap between the chip and the underfill, perhaps related to the high humidity uptake of this material. Note the crack in the bump at left.

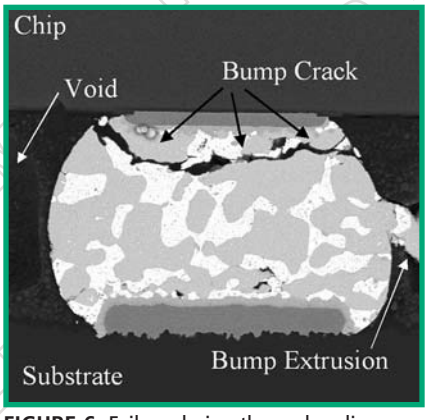

FIGURE 6: Failure during thermal cycling testing of Material C on Solder Mask 1: Bump material has been extruded into an adjacent void, and the bump itself is cracked. A second void is at left.

Delaminations at the die corners were noted after only 24 hours in the pressure cooker; full delaminations and electrical failure happened with all three solder mask types after 96 hours. In thermal cycling, peripheral delaminations from SM 3 were noted after 250 cycles and after 1,000 cycles from SM 1 and SM 2. Electrical failures happened only after 1,500 cycles for SM 1.

Material D

No delaminations were noted after Level 3 testing, but full delaminations and electrical failure occurred after Level 1. Peripheral delaminations were noted after only six hours in the pressure cooker; strong delaminations and partial electrical failure happened with all three solder mask types after 96 hours. In thermal cycling, delaminations from SM 1 happened after 500 cycles and after 1,000 cycles from SM 2; no delaminations occurred from SM3. Electrical failures happened only after 1,500 cycles for SM 1 and SM 2.

Material E

No delaminations were noted after Level 3 testing, but strong to full delaminations and partial electrical failure occurred after Level 1. Slight delaminations were noted after six hours in the pressure cooker. No electrical failures happened after pressure cooker storage. In thermal cycling, first delaminations were noted from SM 1 after 500 cycles; no delaminations occurred from SM 2 and SM 3.

Conclusions

A test matrix of five capillary flow underfill materials and of three solder mask materials has been analyzed using analytical and empirical tools. The study showed that careful material selection for substrate, solder mask and underfiller can yield assemblies with reliabilities of at least 2,000 thermal cycles at –55°C/125°C—which is more than some commonly used surface-mount components can survive.

Flip chip technology is well suited to current production and performance demands. On the horizon are even greater challenges, such as high temperature applications (at 150° and even 200° C) and underchip gaps in some radio frequency (RF) and sensor applications as small as 10 microns. ■

Karl-Friedrich Becker *is with the Fraunhofer Institute, Berlin, Germany; and* ***Tom Adams*** *is a consultant with Sonoscan, Inc., Elk Grove Village, IL; email: info@sonoscan.com.*